JOURNAL OF SPACECRAFT AND ROCKETS
Vol. 40, No. 5, September–October 2003

Numerical Simulation of Titan IVB Transonic Buffet Environment

W. A. Engblom*
The Aerospace Corporation, El Segundo, California 90245-4691

The Titan IVB launch vehicle has experienced much larger than expected buffeting during transonic flight, according to flight telemetry. Computational-fluid-dynamics (CFD) simulations of the unsteady, full three-dimensional, transonic flow environment were conducted to identify the origin of the large vibration levels. Two simulation results are presented, at Mach 0.8 and 1.1, which identify a new, important fluid dynamic mechanism that produces a relatively strong buffet environment. This mechanism involves large vortex pairs, which are periodically shed along the core body. Comparisons between flight data and CFD simulation results demonstrate adequate emulation of both the frequency and magnitude of the unsteady aerodynamic loads. The vortex-pair shedding frequency is shown to be analogous to von Kármán vortex shedding. However, a unique mechanism of instability is proposed. The implications of this work for wind-tunnel testing procedures are also addressed.

Nomenclature

Az	=	azimuthal angle
$C_{p,\mathrm{rms}}$	=	rms pressure coefficient
D	=	diameter
f	=	frequency
M	=	Mach number
P	=	static pressure
Q	=	dynamic pressure
Re	=	Reynolds number
Sr	=	Strouhal number
T	=	temperature
U_∞	=	freestream velocity
α	=	angle of attack
β	=	sideslip angle

Introduction

TELEMETRY data taken during transonic flight of several Titan IVB vehicles have suggested that the buffet environment (i.e., the unsteady aerodynamic flow) is significantly stronger than expected. For example, during ascent of Titan IVB flight vehicle B-27, a pitch-direction accelerometer located on the aft skirt (or boat tail) of the payload fairing (see Fig. 1) registered 17-Hz vibration levels that were two times larger than predicted. Note that the Titan IVB consists of a central core body, flanked by two solid rocket motors. This event occurred at approximately 43 s after liftoff (i.e., $t + 43$ s), just after the vehicle reached sonic speed (i.e., $M = 1.1$). Several vehicles experienced similar pitch-directed vibrations during near-sonic flight.

Various external pressure transducer signals taken aft of this accelerometer (i.e., along the stage 2, core vehicle surface) also indicated larger than expected surface-pressure fluctuations throughout transonic flight. Note that stage 2 consists of three compartments: 2A, 2B, and 2C (see Fig. 1). For example, along compartments 2A and 2B, which typically encounter the largest unsteady pressure levels on the vehicle, the maximum $C_{p,\mathrm{rms}}$ at a given Mach number are typically two to three times higher in flight than predicted in the Titan IV wind-tunnel program. An explanation for this deficiency will be provided later.

The buffet forcing functions for much of the U.S. launch vehicle fleet (e.g., Delta II, Titan IV, and shuttle) were derived from wind-tunnel buffet test programs involving subscale models. For the Titan IV buffet test program,[1] a 7.9% truncated model of the vehicle was used. The truncated model does not include an aft portion of the vehicle. The model was instrumented with high-frequency pressure transducers at various positions along the vehicle surface. The resulting pressure signals for a given test condition were converted into full-size vehicle signals, which were then integrated to provide a buffet forcing function over the entire vehicle surface.

Flight data are typically used to refine the buffet forcing function predictions. However, because of limitations on telemetry bandwidth, it is difficult to resolve adequately the buffet environment during a single flight. Consequently, the accuracy of the wind-tunnel data is often crucial for the accurate prediction of structural loads well past a vehicle's maiden launch.

Unfortunately, subscale wind-tunnel tests might not always resolve significant features of the buffet environment. It will be shown in the Discussion section that the Titan IV wind-tunnel test transducer locations did not allow characterization of the "hot spots" (the regions of largest amplitude pressure fluctuations). It is also speculated that seemingly minor differences between the wind-tunnel test model and flight vehicle might have contributed to flow resolution difficulties.

A major difficulty in performing accurate buffet tests is that the primary buffet load mechanisms for multibody launch vehicles are not well understood. It is very difficult to configure a limited set of pressure transducers to capture accurately a vehicle's buffet "hot spots" without a fundamental understanding of the buffet mechanisms.

Computational fluid dynamics (CFD) is used here to study the transonic flowfield of the Titan IVB. Recent advances in parallel computing have made transient simulation of the Titan IVB buffet environment feasible with standard numerical algorithms. Steady flowfield solutions have been obtained by Wang et al.[2] and J. Bomba (private communication, Sept. 2000). These solutions clearly identify the presence of weak, bound longitudinal vortex pairs on opposite sides of the core at Mach numbers between 0.6 and 1.6. A portion of this flow that passes behind the payload fairing is accelerated toward the core because of the presence of the solid rocket motor upgrade (SRMU) booster noses. This crossflow results in the roll up of the vortex pairs along the core body. It will be shown later that this vortex-pair region is actually unstable and produces strong alternate vortex-pair shedding that can be captured analytically, provided the computation involves fine enough spatial resolution.

Received 31 October 2001; revision received 15 December 2002; accepted for publication 10 January 2003.

*Engineering Specialist, Fluid Mechanics Department, Vehicle Systems Division, 2350 E. El Segundo Boulevard; william.a.engblom@aero.org. Senior Member AIAA.

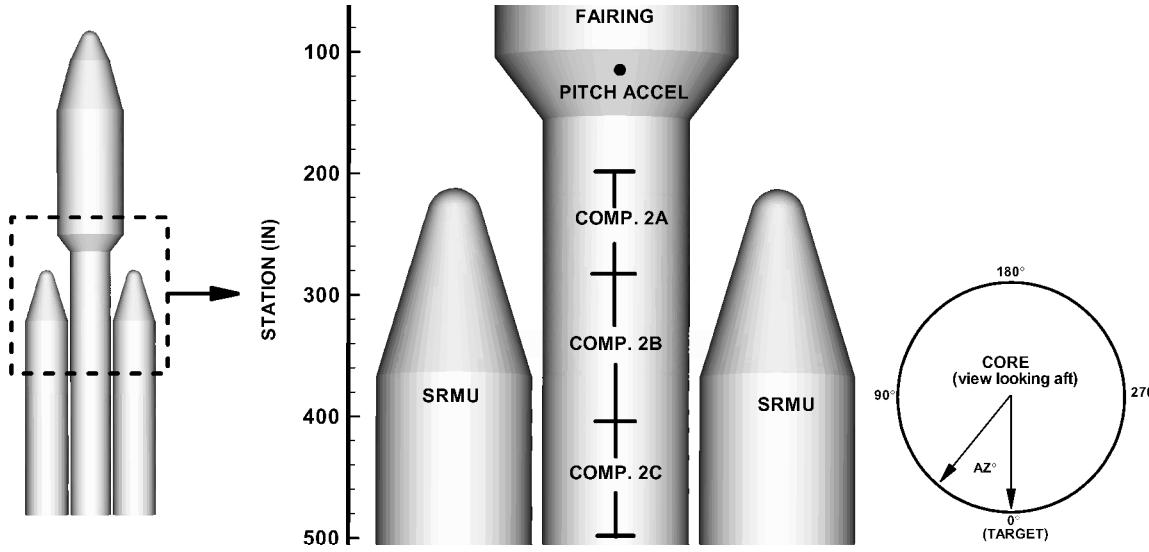

Fig. 1 Titan IVB solid-body model.

There have been only a few attempts to numerically simulate the buffet environment of an actual three-dimensional vehicle. The first successful attempt, by Rizk et al.,[3] was the simulation of the F-18 aircraft tail buffet environment. Several others have also simulated F-18 tail buffet with increasing model complexity. Most recently, Sheta and Huttsell[4] characterized the strong coupling of the F-18 vertical tail motion with the unsteady aerodynamic flowfield and made extensive comparisons to experimental and flight data.

The main objectives of this work are 1) to improve our general understanding of buffet load mechanisms for multibody launch vehicles and 2) to explain the anomalous structural responses observed during Titan IVB ascent. This work represents the first attempt to simulate numerically the unsteady transonic environment for the Titan IVB launch vehicle.

Methodology

A computationally intensive CFD approach is taken to simulate the Titan IVB buffet environment. The full three-dimensional, unsteady Navier–Stokes equations are integrated in a time-accurate manner. No symmetry planes are used. Both thin-layer and cross-derivative laminar viscous terms are included, but turbulence is omitted. The grid is thought to be exceptionally well resolved in the inviscid region along stage 2. The main idea is to capture the low-frequency transonic flow features that are evident in the flight data. The energy in the buffet environment hot spots, according to flight data, is concentrated below 50 Hz. It is not clear whether further simplifications to the model are appropriate.

Model Geometry

A truncated, three-dimensional Titan IVB surface geometry is modeled. A solid body model (Fig. 1) for Titan IVB was constructed in I-DEAS, a CAD software licensed from Structural Dynamics Research Corp. The aft portion of the vehicle, including nozzles, was truncated from the computational domain to reduce computational expense. Based on flight data, the primary buffet behavior was expected to occur along the core vehicle, between the boat tail and approximately the first third of the solid motors. Reflections from the downstream boundary are not expected to influence significantly the upstream flowfield because the freestream is either near or above sonic speed in the simulations. Based on the relatively small amplitude vibrations measured in flight, the coupling between the vehicle and unsteady flowfield is expected to be negligible. Consequently, the vehicle structure is assumed rigid. The long, thin cylindrical structural members that connect the core to each of the two boosters (not shown in Fig. 1) are also neglected based on a Strouhal argument. That is, the primary frequency of the noise generated by these nearly cylindrical bars would be in excess of 400 Hz for the flight conditions considered here, compared to the target frequency range of less than 50 Hz.

Grid Resolution

A review of available telemetry hinted at the presence of alternate vortex shedding across the stage 2 core cylinder. Consequently, the flowfield resolution was chosen based on standards suggested by previous research involving vortical flows. Grasso and Iaccarino[5] have suggested criteria for resolving the steady vortex flow around a supersonic missile at various angles of attack using both the laminar, Navier–Stokes equations and the turbulent, Reynolds-averaged Navier–Stokes (RANS) equations. Specifically, a resolution normal to the surface on the order of 0.01 diameters and an azimuthal resolution along the surface of 1–3 deg were proposed. Applying these criteria results in resolutions of roughly 1 in normally and 2 in circumferentially along the Titan IVB core surface ($D = 100$ in.). A 2-in. longitudinal resolution was also chosen arbitrarily (along the stage 2 core). Based on these resolution parameters, the first grid (grid 1) contains approximately 4 million cells (~50% in the region of interest along stage 2) and 175 blocks. The grid coarsens azimuthally and longitudinally by a factor of two at a "safe" radial distance away from the core vehicle. The mesh was developed using ICEM-CFD, a commercial software licensed by ICEM-CFD.

A similar grid (grid 2) was constructed to reduce the grid size while maintaining nearly the same resolution criteria. The most important change was that the average longitudinal resolution criterion was increased to 3-in. increments from 2 in. This grid has approximately 2.5 million cells. Sections of grid 2 are provided in Fig. 2. A coarse version of this grid (i.e., $\frac{1}{2}$ resolution in all three directions and ~300,000 cells) was also utilized in a cursory grid sensitivity study. Note that a conventional grid resolution study was not performed because of heavy computational requirements but will be attempted in future work.

Freestream Conditions

Two points along the Titan IVB trajectory were simulated. The state vectors are summarized in Table 1. The two trajectory points are at $\sim T + 36$ s (i.e., $M = 0.8$, altitude 12.5 kft) and $\sim T + 43$ s (i.e., $M = 1.1$, altitude 19.8 kft). Level flight is assumed in both cases.

The first point was chosen because the telemetry data indicated strong vortex-shedding type behavior in compartment 2C. The second was chosen because telemetry indicated the largest vibration levels for the Titan IVB vehicles at ~17 Hz (described earlier). The first and second simulations were performed utilizing grids 1 and

Table 1 Simulated freestream conditions

Parameter	Case 1	Case 2
M	0.80	1.10
T, R	474	449
P, psi	9.2	6.8
Q, psi	4.1	5.8
α, deg	0	0
β, deg	0	0

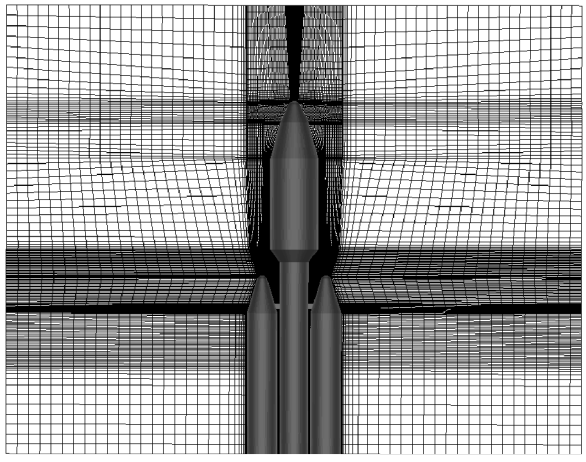

a) Yaw plane for entire domain

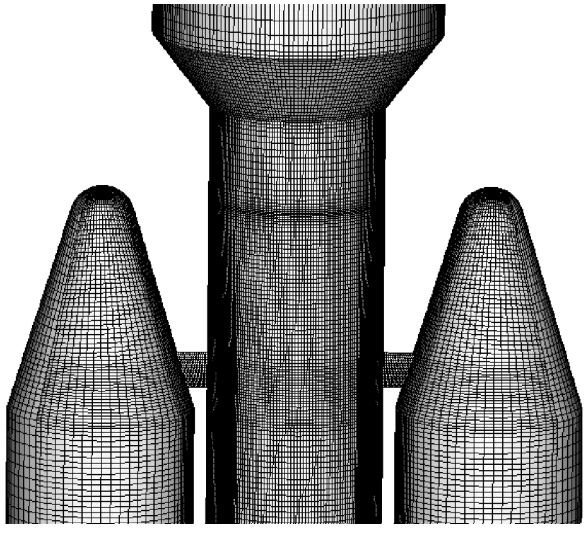

b) Titan IVB surface only

Fig. 2 Sections from grid 2.

2, respectively. These two cases also illustrate how the flowfield changes during the most intense portion of transonic buffet.

Flow Solver

The commercial CFD code, General Aerodynamic Simulation Program (GASPv3), licensed by Aerosoft, Inc., was chosen as the flow solver for this effort. GASPv3 (Ref. 6) is a versatile, finite volume, multiblock, structured-mesh code. Features of GASP deemed essential to the timeliness of the simulations include arbitrary grid distribution across block boundaries, parallel (shared-memory) processing compatibility, and compatibility with the ICEM-CFD grid generator.

The implemented numerical scheme to solve the full Navier–Stokes equations is second-order accurate in space and time. The inviscid fluxes were computed with Van Leer flux-vector splitting,[7] plus upwind biasing, to capture strong inviscid flowfield gradients. Min-mod limiters were used to ensure monotonicity in the solution (i.e., to satisfy the total-variation-diminishing property). An explicit, two-step, Runge–Kutta algorithm was chosen for time-accurate computation. All viscous terms (both thin layer and cross derivative) are computed via central-differencing. The downstream outflow boundary conditions (i.e., one-dimensional Riemann invariant for the Mach 0.8 case; extrapolation for the Mach 1.1 case) were chosen to minimize reflections toward the upstream.

Numerical Procedure

Each simulation starts with a uniform flowfield equivalent to the freestream conditions. After approximately half a second of simulated real time, the solutions develop strong, self-sustained oscillatory behavior along the stage 2 core. Each simulation was conducted for approximately 1 full second of physical time. As described later, a strong vortex-pair shedding mechanism is captured in each case. Note that the transient solution in each case did not become completely repeatable (i.e., pseudosteady) after 1 s of simulation. However, the rms and frequency content of the primary pressure fluctuations do become essentially constant in each case, and the qualitative character of the unsteady flow also appears to be constant.

The simulations were computationally intensive. The maximum allowable time step was typically 10^{-5} s. Because approximately 1 s of real-time simulation was conducted, each simulation required 10^5 steps. Each simulation required roughly two months of computation using 16 processors on a shared-memory Origin 2000, or 20,000 CPU hours.

Numerical Assumptions

A primary, simplifying assumption of this work is that of laminar flow. This assumption is necessary to eliminate the heavy computational requirements (i.e., stiffness) associated with turbulence modeling. There is also concern that a RANS approach, which is based on the time-averaged Navier-Stokes equations, might dissipate the true temporal behavior of the flowfield. Finally, it is assumed that turbulent boundary-layer and shear-layer effects are not primary drivers of the low-frequency buffet environment. Note that the primary buffet load mechanism is ~17 Hz, based on available flight data. This "target" frequency is orders of magnitude lower than the scale of the turbulent eddy energy. The present calculation can be considered an underresolved direct numerical simulation, limited to resolving very large-scale turbulent structures.

Research on vortex formation over missiles at high angle of attack[5] has demonstrated a minor role of turbulence. The reason given is that, at high angle of attack, vorticity production caused by turbulence effects is minor compared to that created via crossflow acceleration (i.e., the influence of the missile geometry). Because it was expected that the primary buffet environment mechanism for the Titan IVB is related to this geometry-related vorticity production, it is reasonable to suspect that wall turbulence will be only a modest effect.

The omission of turbulence effects also assumes that turbulence does not significantly affect the structure of the flowfield. Admittedly, this assumption is tenuous because turbulence intensity has been shown to affect modestly the size and shape of recirculation regions at low-speeds. For example, it has been shown experimentally that increased freestream turbulence levels for low-speed flow over a rearward-facing step shortens the recirculation region, moving the reattachment position forward.[8] For the Titan IVB it is assumed that the shape of the large separated flow region aft of the boat tail is not strongly affected by the omission of a turbulence model.

Results for Case 1 (Mach 0.8)

A map of the relative strength of the predicted buffet environment along the Titan IVB surface is illustrated in Fig. 3. Specifically, the contours represent the rms pressure fluctuations during the last ~0.24 s of the simulation. Note that the ordinate provides the station (i.e., longitudinal vehicle location). The time interval is only approximately three cycles of the primary fluid dynamic feature, to be described next. Note that the other half of the vehicle surface (not shown) is almost identical to Fig. 3. The lack of symmetry in the solution is mainly attributed to the limited sample interval of

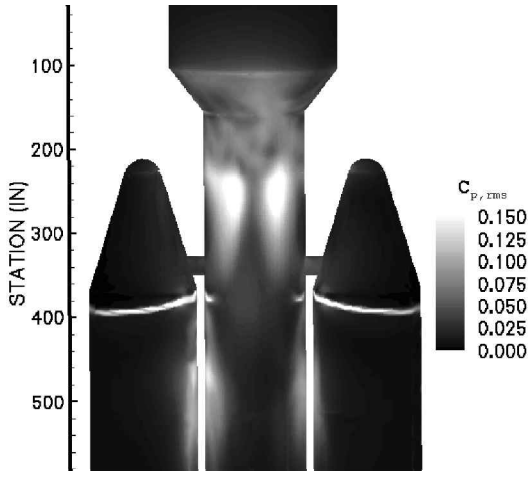

Fig. 3 Map of rms pressure loads at Mach 0.8.

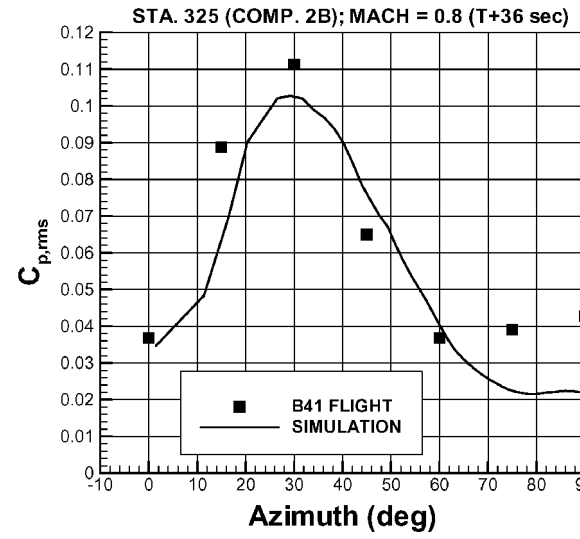

a) Station 325

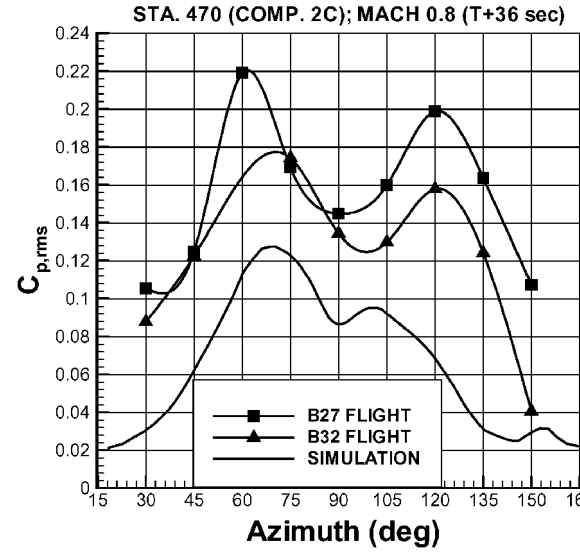

b) Station 470

Fig. 4 Comparison of flight data vs simulation near hot spots at Mach 0.8.

~0.24 s. Also, repeatable surface-pressure oscillations were not attained by the end of the simulation. Note that it has been verified that the multiblock grid is completely symmetric in size and distribution. Consequently, a much longer time interval (e.g., 2 s) might be necessary to achieve symmetric results.

A direct comparison of pressure transducer telemetry data along the stage 2 core with the "virtual" transducer readings demonstrates good qualitative and quantitative agreement. Figures 4a and 4b illustrate comparisons of Titan IVB flight vs simulation data for sets of transducers taken at station 325 (in compartment 2B) and station 470 (in compartment 2C), respectively. The station 325 readings are along the aft edge of the primary hot spot of the buffet environment at Mach 0.8, as predicted by the simulation. The simulation and flight data exhibit similar peak rms pressure levels and azimuthal distribution. Specifically, peak $C_{p,\mathrm{rms}}$ levels of roughly 0.1 occur at an azimuth of roughly 30 deg. The station 470 readings are close to the secondary hot spot, and the simulation underpredicts the magnitude by about 50% while exhibiting a similar azimuthal distribution. The flight data are far from symmetric. The latter is probably as a result of asymmetric surface protuberances or winds. Note that the vehicle flight conditions (i.e., Mach number, angle of attack, sideslip) are constantly changing and are expected to have a significant effect on the unsteady aerodynamics. A discussion of the predicted vs recorded frequency content will be provided later. The thin light rings around the SRMUs, just below the cone–cylinder junction, are related to the motion of reattachment shocks.

Alternate Vortex-Pair Shedding Mechanism

The primary hot spots in Fig. 3, along compartments 2A and 2B, are directly attributable to a new alternate vortex-pair shedding mechanism. This alternate shedding represents the dominant transient load mechanism in the simulation. A sequence of the pressure/velocity field along a transverse slice (i.e., at station 310) about halfway down the SRMU nose cones clearly demonstrates its periodic nature (Fig. 5). This mechanism involves vortex pairs, which are alternately shed along the core vehicle at a nearly constant frequency (~14 Hz for Mach 0.8 case). This mechanism results in a relatively large, unsteady pitch-directed load applied to the Titan IVB core vehicle. Representative pressure signals taken at two surface locations within the primary hot spots are shown in Fig. 6 (both 30 deg from the target azimuth of 0 deg defined in Fig. 1) for the last 0.24 s of the simulation. Both signals are on the same side of the core. The lack of repeatable cycles indicates that the solution is not completely settled.

The primary source of vorticity appears to be related to the strong crossflow acceleration effect created by the vehicle geometry. More specifically, because of the presence of the two SRMU noses a portion of the flow passing the fairing must accelerate toward the core from both sides (i.e., two strong crossflow currents are created). Figure 7 is a typical snapshot of the pressure contours and velocity vectors in this region along a yaw plane slice. A low-pressure (light gray) recirculation region forms behind the boat tail. These two crossflow currents also must bifurcate upon reaching the core, resulting in four crossflow streams. These viscous streams must turn sharply both radially inward towards the core and around the core, while continuing to move downstream. Figure 8 is a snapshot of how the flow "corkscrews" using a rake of three-dimensional ribbons starting near the core surface at station 230. Note that the two streams are moving azimuthally around the core, from each side, and downstream. The underlying contours represent the surface-pressure distribution. The two long, low-pressure (light gray) regions extending downstream along the core body surface are essentially shadows related to the streamwise vortex pairs just off the surface. Note that the shape of the recirculation region, which is highly transient, also can influence the vorticity production. Finally, it is possible that crossflow vorticity generated in the recirculation region behind the hammerhead fairing is intermittently turned and convected downstream to create the streamwise vorticity, although no clear evidence of such an effect was discovered.

As for the natural unsteadiness, animations of the transient flowfield along the pitch plane suggest a plausible explanation. Three pitch plane shapshots, each separated by roughly a $\frac{1}{4}$-cycle, are provided in Fig. 9. This plane cuts longitudinally between the vortex pairs, the effects of which are highlighted. The low-pressure (light

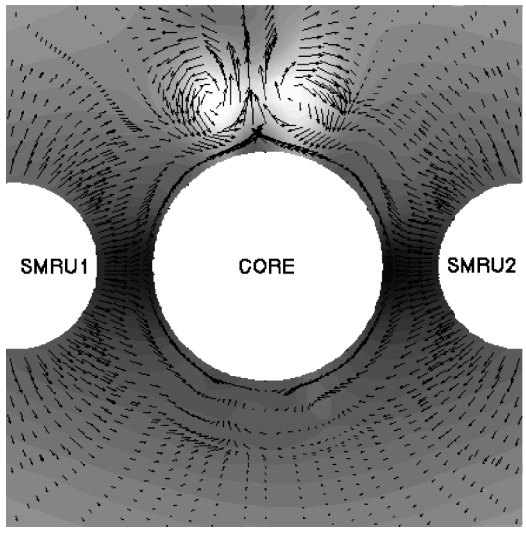

a)

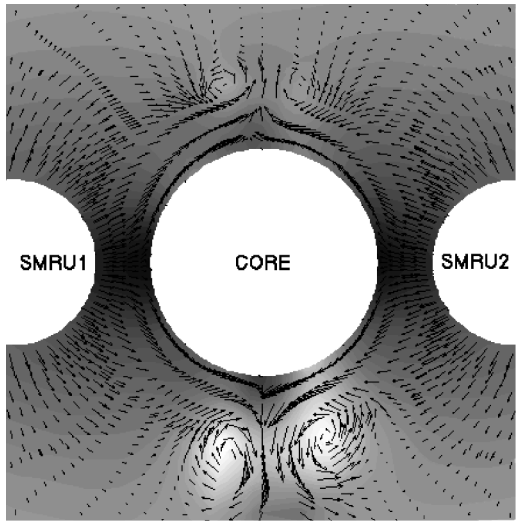

b)

Fig. 5 Snapshots of pressure contours illustrating alternate vortex shedding sequence at Mach 0.8: a) pair of vortices (light gray region) and b) new pair of vortices on opposite side of core vehicle (0.035 s later).

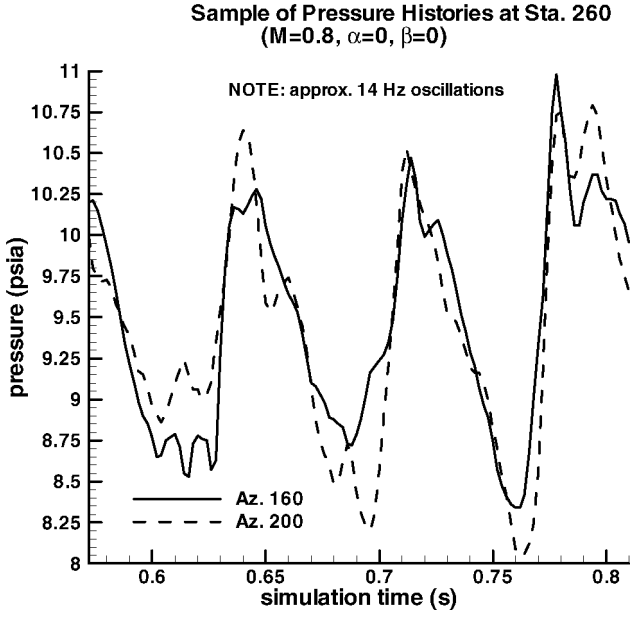

Fig. 6 Sample of pressure signals within compartment 2A.

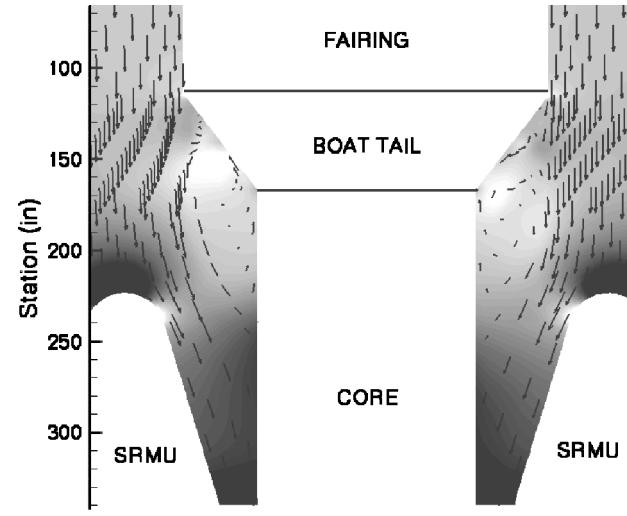

Fig. 7 Snapshot of yaw plane pressure contours for Mach 0.8 case; light contours, low pressure; vectors, magnitude and direction.

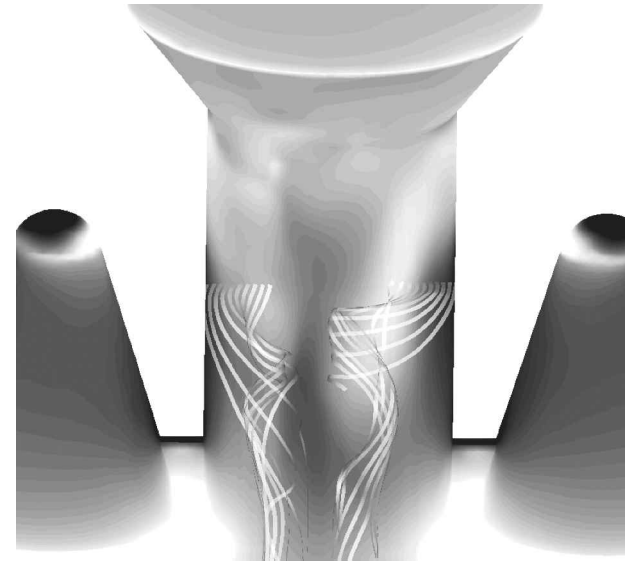

Fig. 8 Illustration of vortex pairs using three-dimensional ribbons and surface-pressure contours for Mach 0.8 case: light contours, low pressure.

gray) vortex-pair regions (see Fig. 9a) are not to be confused with the low-pressure, crossflow vortices created within the recirculation region upstream. Note that the vortex pairs act as obstructions to the freestream flow, causing the large, high-pressure (dark gray) region to form immediately upstream as a result of the inviscid interaction. This high-pressure region moves downstream with the vortex pair. A strong vortex also forms within the recirculation region just upstream of this high-pressure region. The vortex pair "lifts-off" the core surface as it convects downstream (see Fig. 9b). This liftoff effect is expected because of the proximity and vorticity vectors of the vortices. The crossflow vortex just aft of the boat tail has convected downstream somewhat during the $\frac{1}{4}$-cycle interval. The freestream flow is subsequently diverted more strongly toward the opposite side of the core, where a new pair of vortices is formed at the $\frac{1}{2}$-cycle interval (see Fig. 9c). This process repeats itself periodically.

This alternate vortex-pair shedding mechanism can occur only for specific vehicle geometries. In the present time-accurate solutions for the Titan IVB, these strong streamwise vortex pairs form and convect along the core body nearly periodically. However, a similar numerical analysis conducted for a vehicle similar to the Titan IVB in level flight, but without a hammerhead (i.e., fairing diameter equal to the core diameter), indicates only the presence of

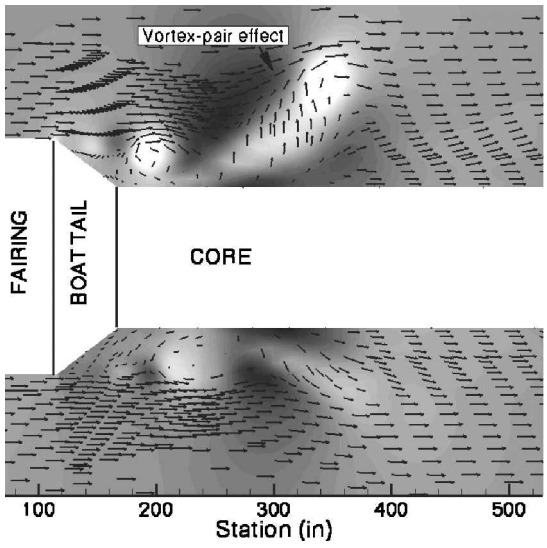

a)

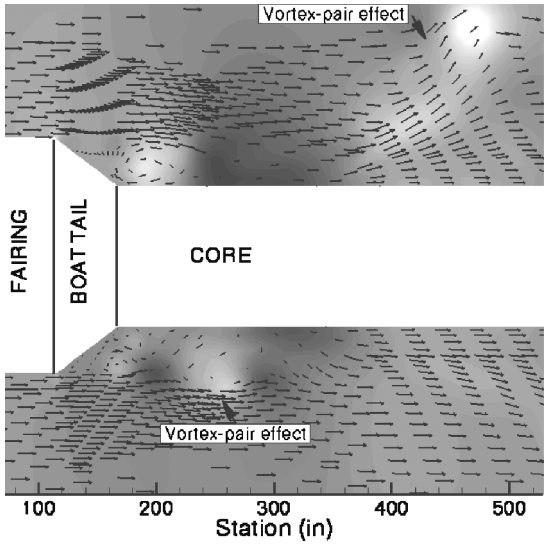

b)

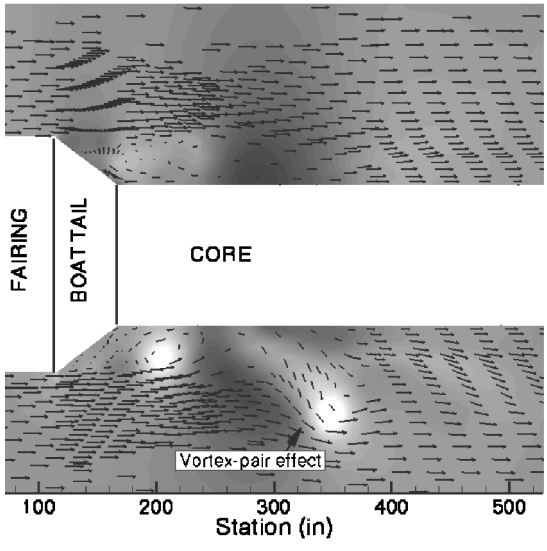

c)

Fig. 9 Pitch plane pressure contours for Mach 0.8 case; a) strong vortex-pair effect on top, b) $\frac{1}{4}$-cycle later, and c) $\frac{1}{2}$-cycle later with strong vortex-pair effect on bottom (light contours, low pressure; vectors, magnitude and direction).

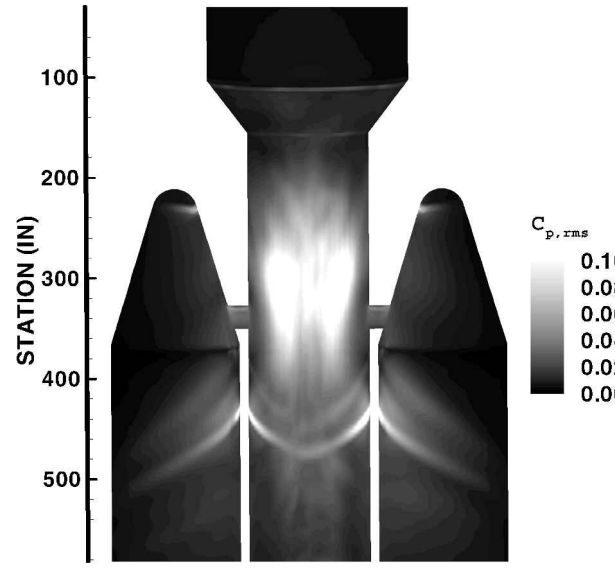

Fig. 10 Map of rms pressure loads at Mach 1.1.

weak, steady vortex pairs on both sides of the core body. Clearly an axisymmetric core body alone, without the two boosters, could not produce similar streamwise vortex pairs, regardless of the fairing configuration. Consequently, it appears that both the oversized fairing (i.e., hammerhead) and boosters must be present to produce this strong transient phenomenon.

Results for Case 2 (Mach 1.1)

A map of the relative strength of the predicted buffet environment along the Titan IVB surface at Mach 1.1 is illustrated in Fig. 10. The contours represent the rms pressure fluctuations during the last ~0.5 s of the simulation (for a 1.2-s computation). The time interval is approximately 10 cycles of the primary vortex-shedding mode, which is at ~21 Hz. Again, the other half of the vehicle surface (not shown) is almost identical. The modest lack of symmetry in the solution is caused by the limited sample interval of 0.5 s. Again, the grid has been carefully constructed to be completely symmetric.

A direct comparison of pressure transducer telemetry data along the stage 2 core with the virtual transducer readings demonstrates good qualitative and quantitative agreement. Figures 11a and 11b illustrate comparisons of Titan IVB flight vs simulation data for sets of transducers taken at station 325 (in compartment 2B) and station 470 (in compartment 2C), respectively. The station 325 readings are near the heart of the primary hot spot of the buffet environment at Mach 1.1, and the simulation predicts similar rms pressure levels and azimuthal distribution. Specifically, peak $C_{p,\mathrm{rms}}$ levels of roughly 0.15 occur at an azimuth of roughly 30 deg. The station 470 readings are close to the secondary hot spot, and the simulation underpredicts the magnitude by about 50% while exhibiting a similar azimuthal distribution. The flight data are not symmetric because of several factors including the effect of winds and asymmetric surface protuberances.

Vortex-Pair Shedding Frequency Content

A waterfall plot (power spectral density vs time) of a pressure transducer signal, from flight telemetry, located in compartment 2B at station 325 and azimuth of 30 deg is provided in Fig. 12. As described earlier, this location is near the heart of the largest loads generated by the vortex-shedding mechanism. Note that Mach 0.8 and Mach 1.1 occur at approximately T + 38 and T + 46 s, respectively, for this flight. Two lines have been drawn through the highest energy levels, which indicate the presence of two modes. It is argued next that these two modes are likely the primary and first harmonic frequencies of the vortex-pair shedding mechanism. There also appears to be a third line in the flight data at higher frequencies (not drawn). It is not clear what mode this line represents.

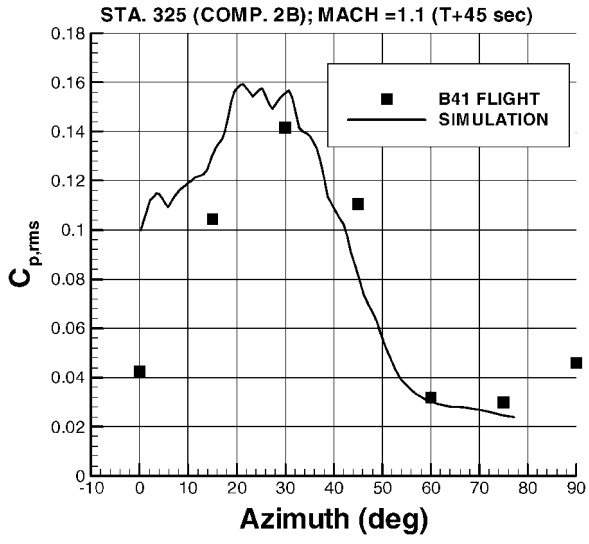

a) Station 325

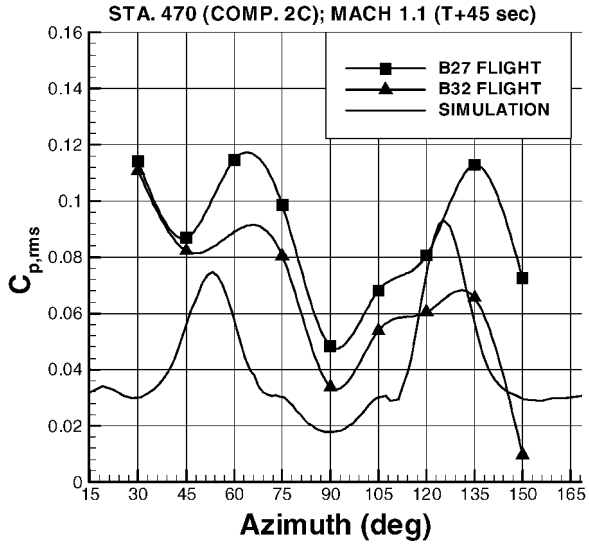

b) Station 470

Fig. 11 Comparison of flight data vs simulation near hot spots at Mach 1.1.

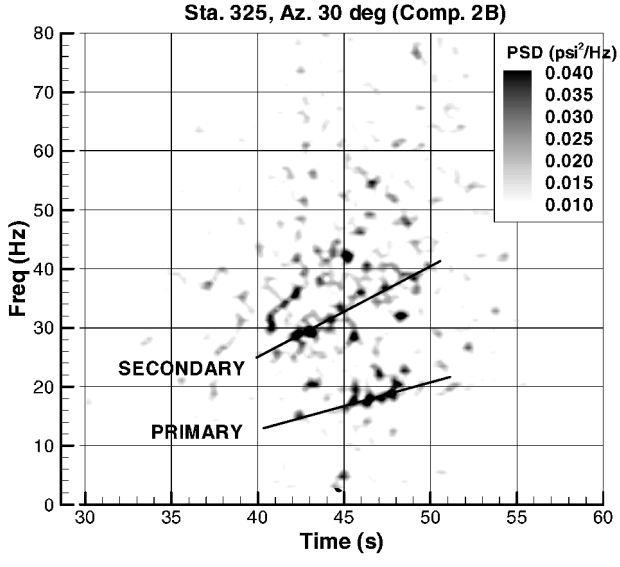

Fig. 12 Power spectral density (PSD) history for pressure transducer in compartment 2B (Titan flight B-41).

Table 2 Vortex-pair shedding primary frequency

Mach	Flight data, Hz	Simulation, Hz
0.8	12[a]	14
1.1	17	21

[a]Projected value (see Fig. 9).

A direct comparison of the primary frequency content of the flight data with simulation results (Table 2) indicates reasonable agreement. The simulation results predict approximately 20% higher frequency than expected based on the flight data. Both the flight data and simulation results also indicate an increase in shedding frequency with freestream Mach number (and velocity), analogously to von Kármán vortex shedding over a cylinder.

These frequencies also suggest near constant Sr numbers of roughly 0.14 and 0.17, for the flight data and simulation results, respectively. The Strouhal number is calculated from Eq. (1) based on the core diameter ($D = 10$ ft) and freestream velocity ($U_\infty = 850$ ft/s at Mach 0.8 and 1150 ft/s at Mach 1.1):

$$Sr = fD/U_\infty \tag{1}$$

These Strouhal values are relatively close to those for von Kármán vortex shedding. Depending on the Reynolds number, strouhal number varies between 0.17 ($Re = 100$) and 0.30 ($Re = 10^7$) for flow over a cylinder, with $Sr = 0.2$ for a large portion of the Reynolds-number range.[9] However, because this vortex-pair shedding mechanism is different from von Kármán vortex shedding it might not be appropriate to make such a comparison. The choices for the reference length and velocity in Eq. (1) are arbitrary.

Power spectral density vs frequency plots for virtual signals taken in both the primary and secondary hot spots are provided in Figs. 13 (Mach 0.8) and 14 (Mach 1.1). The primary modes of ~14 Hz (Mach 0.8) and ~21 Hz (Mach 1.1) are evident in both hot spots. The primary mode of the vortex-pair shedding is dominant at Mach 0.8 (~14 Hz). The first harmonic at Mach 0.8 (~28 Hz) is more significant in compartment 2C than in compartment 2A. The primary (~21 Hz) and secondary (~42 Hz) modes of the vortex shedding are almost equally strong in the Mach 1.1 simulation. Again, the harmonics become more important in the secondary hot spot, compartment 2C.

Discussion

Anomalous Vibrations

As mentioned earlier, unexpectedly large vibrational levels have been measured during ascent of the Titan IVB. Specifically, large pitch-directed vibrations of the core vehicle typically occur around Mach 1.1 and at ~17 Hz for vehicles including a specific upper stage. Significant vibrations at slightly lower frequency vibrations have also been recorded.

A strong case is made next that these pitch vibrations are caused by the alternate vortex-shedding mechanism occurring along stage 2. First, the alternate vortex-shedding frequency is predicted to be roughly 17 Hz during transonic flight. As already discussed, both flight data and the two simulations indicate that the primary frequency increases during the transonic flight regime. Consequently, the aforementioned 17-Hz structural mode present on certain Titan IVB vehicles is excited as the vortex-shedding frequency passes through 17 Hz. Second, according to the simulation results the vortex shedding produces very large, integrated pitch loads with amplitudes of several thousand pounds (over a 50-in. longitudinal segment of the core) and negligible yaw loads. The accelerometer data indicate large pitch vibrations and negligible yaw vibrations. Consequently, the direction of the unsteady loads created by this mechanism is also consistent. Third, the spatial longitudinal distribution of the cyclic pitch force along the core vehicle is also appropriate to excite the specific 17-Hz structural mode (i.e., the modal shape is appropriate). Structural dynamic simulations have recently validated the claim that the alternate shedding is the cause of the anomalous vibrations.[10] These unsteady pitch load magnitudes, if correct, easily represent the largest cyclic loads the Titan IVB vehicle experiences during ascent.

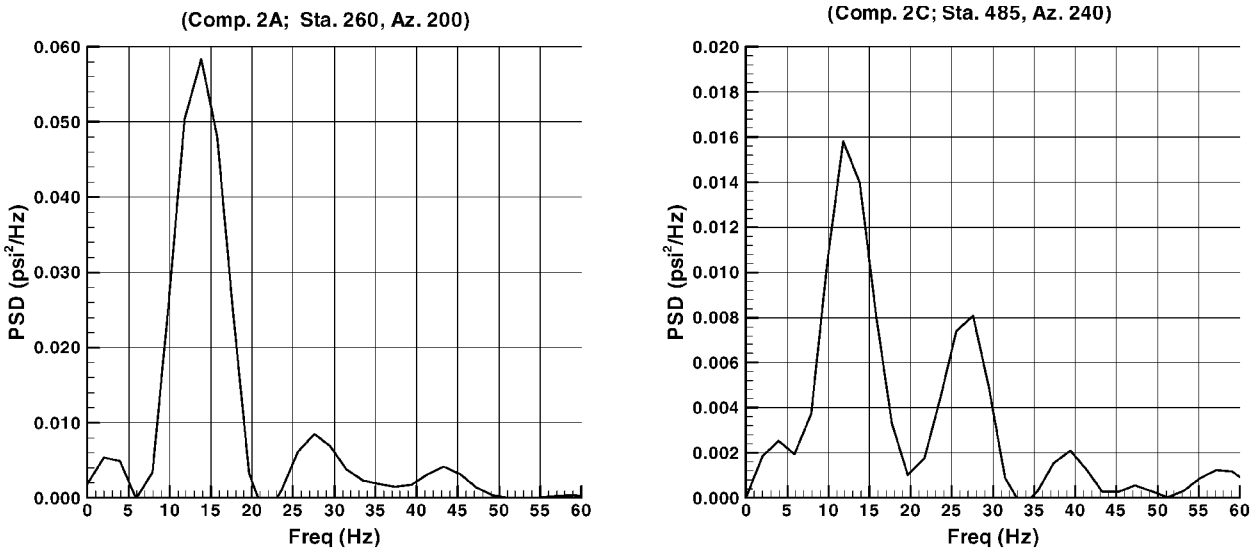

Fig. 13 Representative power spectral density vs frequency based on Mach 0.8 simulation results.

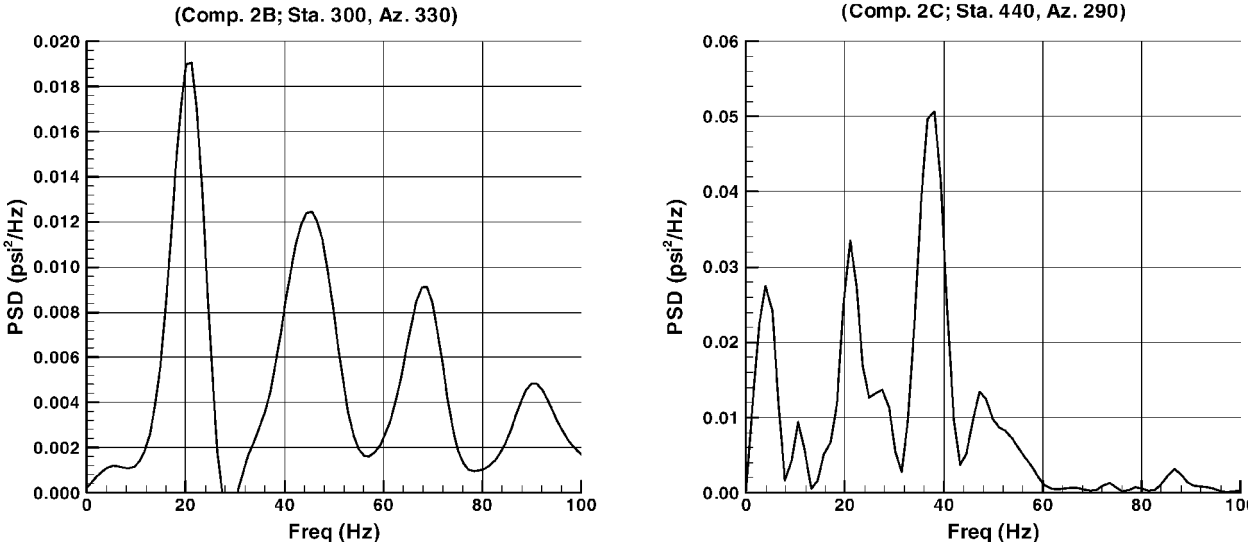

Fig. 14 Representative power spectral density vs frequency based on Mach 1.1 simulation results.

Core/SRMU Gap Flow

The secondary hot spot (compartment 2C) is related to the unsteady flow along the 9-in. gap between the core and SRMU. A large, low-speed, wake structure fills this gap and extends from the SRMU cone/cylinder junction to near the end of the stage 2 core (e.g., in the Mach 0.8 solution this wake extends about 200 in.). The alternate vortex-pair shedding influences this wake flow and to a large extent causes the secondary hot spot. The large vortices spawned in compartment 2A (Mach 0.8) or compartment 2B (Mach 1.1) convect downstream along compartment 2C. The frequency content of the pressure fluctuations in compartment 2C is also similar to that produced by the vortex-pair shedding, as described earlier. It is speculated that the width of the gap has a significant effect on the strength of the unsteady buffet loads in this region.

Implication to Wind-Tunnel Tests

The hot spots illustrated in Figs. 3 and 7 are not easily resolved by wind-tunnel tests. Pressure transducer spacings of 45 or 90 deg, for example, would miss all of the important buffet environment hot spots. The underprediction of rms pressure levels by the Titan IV wind-tunnel test program, discussed in the Introduction, is primarily caused by a lack of pressure transducer resolution. An azimuthal resolution of 15 deg is recommended for similar multibody configurations.

Seemingly minor geometric differences between the Titan IV wind-tunnel model and the actual vehicle might have also had an important effect. The wind-tunnel model was adapted from a Titan IVA model and did not have the correct booster diameter or core/booster gap size. The model also included a large protuberance on the booster nose cones (i.e., jettison motors) not present on the Titan IVB. It is likely that this vortex-pair shedding mechanism is sensitive to such geometric features.

Buffet forcing functions obtained from wind-tunnel testing were scaled up for the full-size Titan IV vehicle by accounting only for the geometric scale. However, vortex-shedding frequency also depends on the velocity scale, per the Strouhal number in Eq. (1). Also, the Strouhal number itself could differ between the flight vehicle and model because of differences in the Reynolds number.

Conclusions

The three-dimensional, transient, transonic flowfield (low-frequency only) encountered by the Titan IVB during ascent has been adequately simulated via the full Navier–Stokes equations. The environment is dominated by a newly discovered low-frequency alternate vortex-pair shedding mechanism. The vortex pairs are alternately shed from the core vehicle at primary and harmonic modes. Root-mean-squared pressure distributions over the vehicle surface based on simulations at Mach 0.8 and 1.1 agree well with flight

data. Both simulation and flight data indicate the presence of the primary and harmonic modes, which increase in frequency with freestream velocity, analogous to von Kármán vortex shedding. The physical mechanism behind the instability is postulated to involve an inviscid-type interaction between the vortex pairs and the oncoming freestream.

Acknowledgments

This work was supported by the U.S. Air Force Materiel Command, Space and Missile Systems Center, under Contract F04701-00-C-0009. The author thanks the Aeronautical Science Center (ASC) Major Shared Resource Center (MSRC) at Wright–Patterson Air Force Base, Ohio, for providing the necessary computational resources for this work. This effort could not have been conducted in a timely manner without the support of the ASC MSRC. The author also thanks Kirk Dotson, Devon Johnson, Young Kim, Earl Parker, Jason Stout, and Mike Weaver for significant technical contributions. Finally, the author thanks Richard Lung, James E. Bartosik, and Mike Zambrana for enabling the necessary funds and support for this research effort.

References

[1]Black, J. A., "A Wind Tunnel Investigation of the Buffet Characteristics of Truncated 0.079-Scale Models of the Titan III and Titan IV Launch Vehicles at Mach Numbers from 0.60 to 1.60," Arnold Engineering Development Center, AEDC-TSR-88-P25, Arnold AFB, TN, Oct. 1988.

[2]Wang, J. C. T., Than, P. T., and Widhopf, G. F., "Multi-Body Launch Vehicle Flowfield Simulation," AIAA Paper 91-0072, Jan. 1991.

[3]Rizk, Y., Guruswamy, G., and Gee, K., "Numerical Investigation of Tail Buffet on F-18 Aircraft," AIAA Paper 92-2673, April 1992.

[4]Sheta, E. F., and Huttsell, L. J., "Numerical Analysis of F/A-18 Vertical Tail Buffeting," AIAA Paper 2001-1664, April 2001.

[5]Grasso, F., and Iaccarino, G., "Influence of Crossflow and Turbulence on Vortex Flow Around a Supersonic Missile," *Journal of Spacecraft and Rockets*, Vol. 35, No. 1, 1998, pp. 37–45.

[6]*General Aerodynamic Simulation Program (GASP) User Manual Version 3*, Aerosoft, Inc., Blacksburg, VA, 1996.

[7]Van Leer, B., "Upwind-Difference Methods for Aerodynamic Problems Governed by the Euler Equations," *Lectures in Applied Mathematics*, Vol. 22, 1985, pp. 266–327.

[8]Castro, I. P., and Haque, A., "The Structure of a Shear Layer Bounding a Separation Region. Part 2. Effects of Free-Stream Turbulence," *Journal of Fluid Mechanics*, Vol. 192, 1988, pp. 577–595.

[9]Schlichting, H., *Boundary-Layer Theory*, 4th ed., McGraw–Hill, New York, 1979, pp. 31–33.

[10]Dotson, K. W., and Engblom, W. A., "Vibration of a Three-Body Launch Vehicle During Ascent," American Society of Mechanical Engineers, Paper IMECE2002-33028, Nov. 2002.

R. M. Cummings
Associate Editor